Journal of Oral Biosciences 61 (2019) 236–241

Contents lists available at ScienceDirect

Journal of Oral Biosciences

journal homepage: www.elsevier.com/locate/job

Technical Note

Dynamic photoacoustic imaging of neurovascular coupling in salivary glands

Laurie J. Rich [a, 1], Eftekhar Rajab Bolookat [a, b], Mukund Seshadri [a, b, c, *]

[a] Department of Oral Oncology, Roswell Park Comprehensive Cancer Center, Elm and Carlton Streets, Buffalo, NY 14263, USA
[b] Department of Radiology-Medical Physics Program, University at Buffalo - Jacobs School of Medicine and Biomedical Sciences, 955 Main Street, Buffalo, NY 14203, USA
[c] Department of Dentistry and Maxillofacial Prosthetics, Roswell Park Comprehensive Cancer Center, Elm and Carlton Streets, Buffalo, NY 14263, USA

ARTICLE INFO

Article history:
Received 23 April 2019
Received in revised form
19 August 2019
Accepted 21 August 2019
Available online 3 September 2019

Keywords:
Salivary glands
Ultrasonography
Pilocarpine
Atropine

ABSTRACT

The purpose of this study was to apply photoacoustic imaging (PAI), a relatively new imaging method, to non-invasively map neurovascular dynamics in salivary glands. Dynamic PAI with co-registered ultrasound (US) was performed in mice to monitor salivary gland hemodynamics in response to exogenous muscarinic receptor stimulation (pilocarpine) and blockade (atropine). Pilocarpine increased salivary gland oxygen saturation (%sO_2) within minutes after administration, which was abrogated by atropine. A significant correlation was observed between change in %sO_2 measured by PAI and saliva secretion. PAI is a novel imaging method that can be used for functional assessment of neurovascular dynamics in salivary glands.

1. Introduction

Saliva is a critical component of the oral microenvironment that facilitates digestion, inhibits bacterial growth, and maintains lubrication of oral tissues [1–3]. Salivary secretion is regulated by sympathetic and parasympathetic arms of the autonomic nervous system under resting and stimulated conditions, respectively [3,4]. This dynamic interaction between the autonomic nervous system and glandular epithelium begins early on during organogenesis and enables maintenance of salivary gland function throughout the life span of an individual [3,4]. Salivary gland cells (acinar and myoepithelial cells) are innervated by both parasympathetic and sympathetic nerves [4,5]. Parasympathetic impulses mediated by acetylcholine or vasoactive intestinal peptide lead to increased salivary secretion, while, sympathetic stimulation mediated by norepinephrine modulates salivary composition and protein secretion [4–6]. Previous studies have demonstrated that disruption of the autonomic nerve supply, especially the parasympathetic arm of the autonomic nervous system, results in marked loss of salivary secretion [3,4,7–9].

The salivary reflex is intrinsically connected to salivary gland blood flow [10–12]. While the relationship between gland hemodynamics and saliva secretion has been of long-standing interest, limited evidence is available on the oxygenation of salivary glands [13,14]. In the present study, we applied photoacoustic imaging (PAI), a relatively new and inexpensive imaging method [15,16], to non-invasively map the neurovascular dynamics of salivary glands in response to exogenous stimulation of the autonomic nervous system. In PAI, near-infrared light is pulsed into the tissues, which results in a localized thermoelastic expansion and generation of pressure waves that are detected acoustically [15,16]. PAI takes advantage of differences in optical characteristics of oxy- and de-oxy hemoglobin (Hb) to provide information on tissue oxygen saturation (%sO_2) [15–17]. In this manner, PAI serves as a hybrid imaging method that builds on the strengths of traditional ultrasound (US) and optical imaging methods to provide images with high contrast and at greater depths.

2. Materials and methods

2.1. Animals

Studies were performed using ten-to-twelve-week-old CB.17 (C.B-Igh-1^b/IcrTac-Prkdc) mice with severe combined

* Corresponding author. Roswell Park Comprehensive Cancer Center, Center for Oral Oncology, Elm & Carlton Streets, Buffalo, NY 14263, USA. Fax: +1-716-845-3118.
E-mail address: Mukund.Seshadri@roswellpark.org (M. Seshadri).
[1] Present affiliation: Center for Magnetic Resonance and Optical Imaging, Department of Radiology, University of Pennsylvania, PA 19104.

https://doi.org/10.1016/j.job.2019.08.002
1349-0079/

immunodeficiency (Laboratory Animal Shared Resource, Roswell Park). Animals were housed in micro-isolator cages in light-controlled rooms and fed house-chow diet. All procedures were performed under institutionally approved protocols.

2.2. Drugs

Pilocarpine hydrochloride (Sigma Aldrich, St. Louis, MO, USA) was administered at 10 mg/kg or 20 mg/kg by intraperitoneal (i.p.) injection. Atropine (atropine sulfate salt monohydrate, Sigma Aldrich, St. Louis, MO, USA) was administered at a dose of 1 μL/g i.p. 10 min prior to pilocarpine administration.

2.3. Photoacoustic imaging with co-registered ultrasound

Experimental imaging was performed using the Vevo® LAZR imaging system (VisualSonics Inc., Toronto, Canada) equipped with a 21 MHz transducer with an axial and lateral resolution of ~75 μm and ~165 μm, respectively. The system enables acquisition of PA images with co-registered US. Animals were anesthetized using 2.5% isoflurane (Benson Medical Industries, Markham, Canada). Hair was depilated over the imaging area and the probe lowered over the salivary gland. B-mode US images were acquired to evaluate salivary gland morphology. Dynamic PA images were acquired before and after the administration of pilocarpine using the following parameters: transducer: LZ-250, depth: 20.00 mm, width: 23.04 mm, wavelength: 750/850 nm, threshold HbT: 20, acquisition: sO_2/Hbt, number of averages: 3. All imaging datasets were analyzed using the Vevo LAB (Ver 1.7.2) workstation software. Average oxygen saturation values of pixels with a $\%sO_2$ estimate, excluding void or zero pixels have been reported [20]. During each imaging session, saliva was collected after every 2 min for 7 min by placing a pre-weighed piece of filter paper into the oral cavity for 90 s, and then, the paper was removed so that it could be re-weighed.

2.4. Histology and immunohistochemistry

Hematoxylin and eosin (H&E) staining and Masson's trichrome (Polyscience; Catalog #K037) immunostaining of glands was performed by the Pathology Network Shared Resource at Roswell Park. Glass slides containing stained sections (4 μm) were scanned and digitized using the ScanScopeXT system (Aperio Technologies, Vista, CA).

2.5. Statistics

The two way analysis of variance (ANOVA) with Tukey's multiple comparisons test was used to compare changes in salivary gland $\%sO_2$ and saliva production levels following pilocarpine injection. Pearson's correlation analysis was used to determine the correlation between saliva secretion and salivary gland $\%sO_2$ following pilocarpine stimulation. A paired *t*-test was used to compare differences in $\%sO_2$ between pilocarpine alone and atropine + pilocarpine (repeated measures within the same cohort).

3. Results & discussion

3.1. Dynamic PAI of neurovascular coupling in salivary glands

Since secretion of saliva is regulated by neural and vascular components, we hypothesized that PAI could serve as a useful tool for temporal mapping of neurovascular dynamics in salivary glands. To test this hypothesis, we developed a novel dynamic PAI method (Fig. 1A) that involved serial image acquisition of murine salivary glands before and after exogenous parasympathetic stimulation using pilocarpine. The anatomy of salivary glands in mice is distinct from humans with the submandibular and sublingual glands forming a large complex in the neck that is separated by connective tissue. In our study, we measured the changes in hemodynamics in this salivary gland complex. Changes in oxygen saturation ($\%sO_2$) of salivary glands were correlated with saliva secretion. The effect of muscarinic blockade on salivary gland hemodynamics was used as a validation measure.

3.2. PAI and correlative histology of murine salivary gland tissue

Ultrasonography is a radiological method that is routinely utilized for assessment of salivary glands in humans [18,19]. However, the potential of PAI for salivary gland imaging has not been extensively studied. We have previously shown that PAI can detect changes in hemodynamics of healthy glands and salivary gland cancers [20]. Building on our earlier work, we examined the correlation between PAI and histology of salivary gland tissue. PAI detected adequate $\%sO_2$ of salivary glands as shown in the pseudo-colorized parametric $\%sO_2$ map in Fig. 1B. Spatially co-registered Masson's trichrome immunostained sections revealed presence of regions containing large vascular structures in the gland (Fig. 1C and D, *white arrows*).

3.3. Dynamic PAI of salivary gland hemodynamic response to pilocarpine

Alterations in blood flow due to various conditions, such as diabetes, have also been shown to affect salivary secretion in mice [21]. Although sympathetic activation can mobilize small levels of saliva, the majority of salivary secretion is mediated through parasympathetic stimulation [11,12]. We therefore investigated the effects of parasympathetic stimulation on salivary gland oxygenation using the muscarinic receptor agonist, pilocarpine. Temporal changes in $\%sO_2$ were measured in mice ($n = 12$) before and after pilocarpine treatment (up to 7 min) using dynamic PAI. Control animals ($n = 4$) were administered saline (~200 μL, i.p.) and PA images were acquired for the same period post-injection. Fig. 2A represents pseudo-colorized oxygen saturation ($\%sO_2$) maps overlaid on B-mode images of the salivary glands before (pre-injection) and at different time points post-pilocarpine administration (1–7 min). No changes in $\%sO_2$ were observed in control animals. In comparison, a steady increase in $\%sO_2$ was observed following pilocarpine treatment over the 7-min imaging period compared to pre-stimulation levels (Fig. 2A and B). The change in $\%sO_2$ in pilocarpine-treated animals was significantly higher ($p < 0.01$ vs. saline at 5 min; $p < 0.001$ at 7 min) than saline controls.

3.4. Correlation between PAI and sialometry

Sialometric measurements showed a similar kinetic response in saliva secretion post pilocarpine treatment (Fig. 2C) with increased volumes at 5 and 7 min post-treatment compared to saline controls ($p < 0.001$) and earlier time points ($p < 0.001$). It should be noted that while our PAI measurements were predominantly focused on the submandibular-sublingual complex, saliva secretion in response to pilocarpine stimulation involves parotid, submandibular, sub-lingual and minor salivary glands. Nevertheless, a significant correlation ($r = 0.9009$, $p < 0.0001$) was seen (Fig. 2D) between the change in $\%sO_2$ levels following pilocarpine administration and stimulated saliva levels validating PAI as an objective measure of salivary function. Our observations are consistent with published reports [13,14,22–25]. In rat

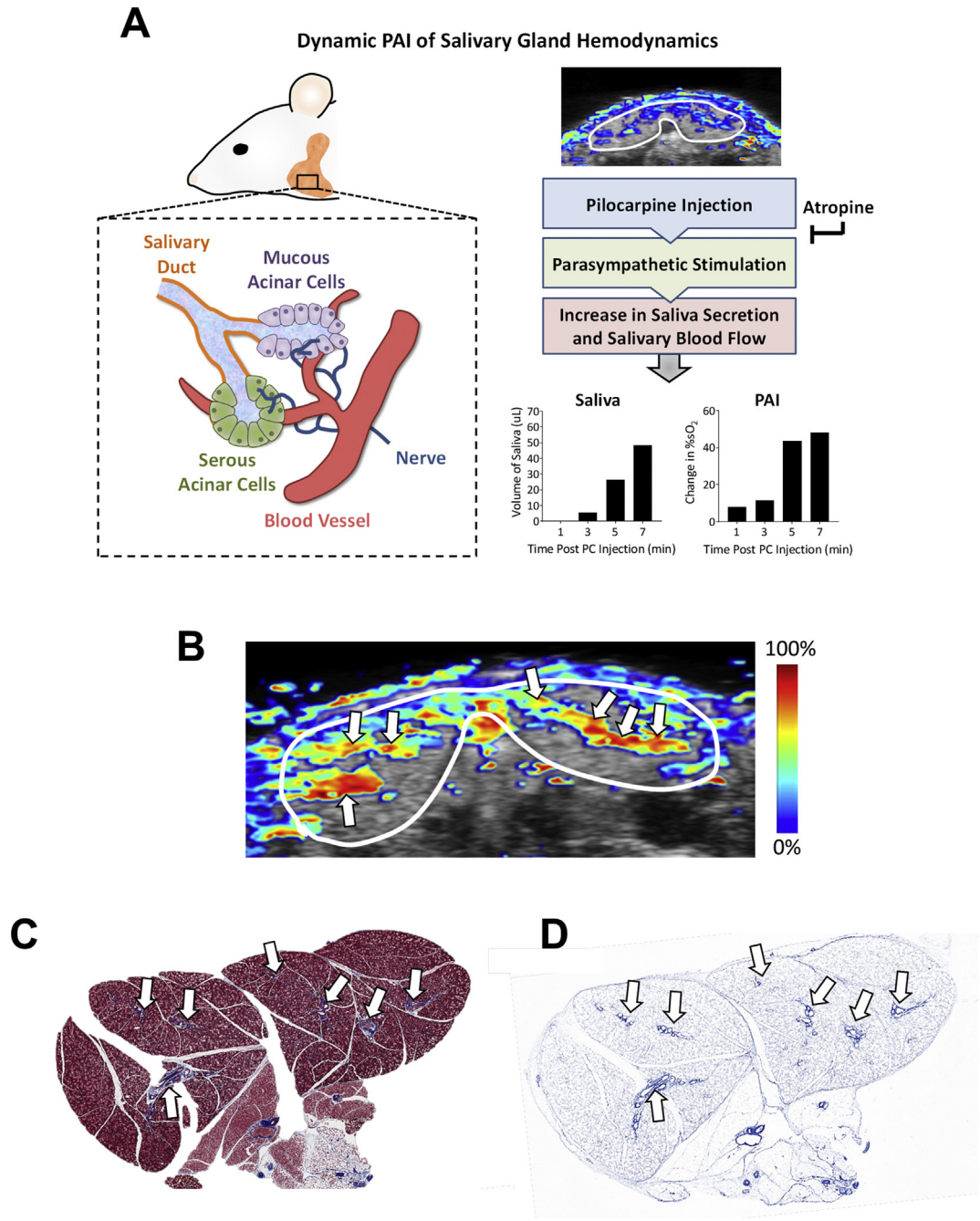

Fig. 1. Dynamic photoacoustic imaging of neurovascular coupling in salivary glands. (A) Schematic illustration of the dynamic PAI method developed for temporal mapping of neurovascular dynamics in murine salivary glands. The method involves acquisition of a series of PA images before and after parasympathetic stimulation using pilocarpine. Changes in $\%sO_2$ were correlated with saliva secretion. The effect of muscarinic blockade (Atropine) was studied to validate the method. Panel of images represent pseudo-colorized oxygen saturation map (B) of healthy murine salivary gland along with co-registered images of Masson's Trichrome staining (C). Threshold image (D) of the immunostained section of the gland is shown to visualize large ducts and vessels (white arrows). Areas of high $\%sO_2$ signal corresponded with regions containing large ductal and vascular structures embedded within connective tissue inside the salivary gland.

submandibular glands, pilocarpine has been shown to increase oxygen uptake that is dependent on Na^+ and Ca^{2+} [14]. Stojic and Terzi have also demonstrated enhanced oxygen consumption by carbachol in rat salivary glands [13]. Using laser Doppler methods, Ono et al. reported increased blood flow following pilocarpine treatment that was associated with salivary secretion [22]. Smaje and Gamble reported a 20-fold increase in blood flow in rabbit salivary glands following parasympathetic stimulation and attributed the effects to a reduction in vascular resistance and increase in capillary surface area that result in increased capillary blood flow [23,24].

3.5. *Effect of atropine on pilocarpine-induced hemodynamic response*

We validated the ability of PAI to detect changes in salivary gland hemodynamics following blockade of parasympathetic stimulation using atropine. Atropine is a parasympatholytic drug

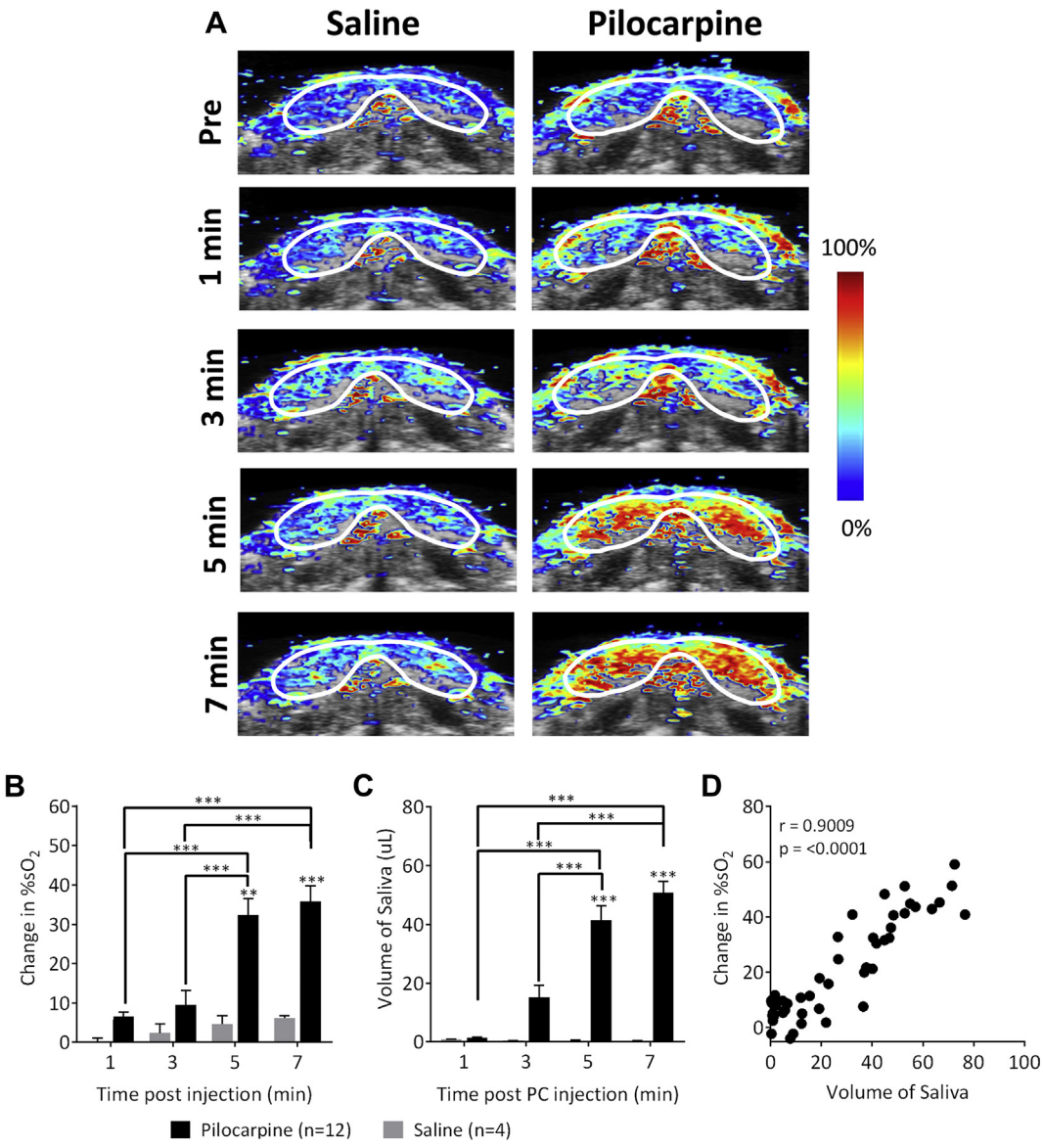

Fig. 2. Dynamic PAI of salivary gland hemodynamic response to pilocarpine. (A) Panel of images represents dynamic series of PA oxygen saturation (%sO_2) maps of salivary glands acquired before (pre-stimulation), and 1, 3, 5, and 7 min after pilocarpine or saline administration. Bar graphs of quantitative estimates of change in %sO_2 levels (B) and salivary secretion (C) at different time points post-pilocarpine administration. (D) Correlation plot comparing temporal change in %sO_2 levels with saliva volume measurements (Pearson r = 0.9009). Error bars represent standard error of the mean. $^{**}p < 0.01$, $^{***}p < 0.001$.

that binds to muscarinic acetylcholine receptors and prevents receptor activation [11,24]. We used PAI to detect changes in salivary gland hemodynamics following administration of pilocarpine in mice with or without pre-treatment with atropine (n = 5). Consistent with our first study, injection with pilocarpine resulted in a visible and quantitative increase in %sO_2 ($p < 0.001$ compared to pre-pilocarpine levels) on PAI (Fig. 3A *top*). Pre-treatment with atropine (1 μL/g body weight) administered 10 min prior to pilocarpine administration almost completely attenuated the changes in %sO_2 induced by pilocarpine. PAI of atropine-treated mice revealed a visual loss in hemodynamic response to pilocarpine stimulation (Fig. 3A *bottom*). Quantification of %sO_2 levels showed a significant reduction beginning at 3 min ($p < 0.01$ or greater) in atropine pre-treated animals (Fig. 3B). Significantly ($p < 0.001$) lower salivary secretion levels were seen in atropine treated animals compared to animals treated only with pilocarpine (Fig. 3C).

4. Conclusion

The current study highlights the utility of PAI as a novel imaging method for functional assessment of neurovascular dynamics in salivary glands. We propose that PAI can serve as a complimentary adjunct to US to assess hemodynamic and secretory function of salivary glands. Compared to technically advanced imaging techniques, such as CT or PET, PAI with co-registered US does not employ ionizing radiation, is easy to perform, and exploits endogenous contrast mechanisms. The rapid acquisition times enables acquisition of dynamic imaging datasets of salivary glands within a short time period (in the order of minutes).

The limitations of our study warrant recognition. First, given the unique anatomy of the mouse salivary glands, we did not obtain individual measurements from each of the major

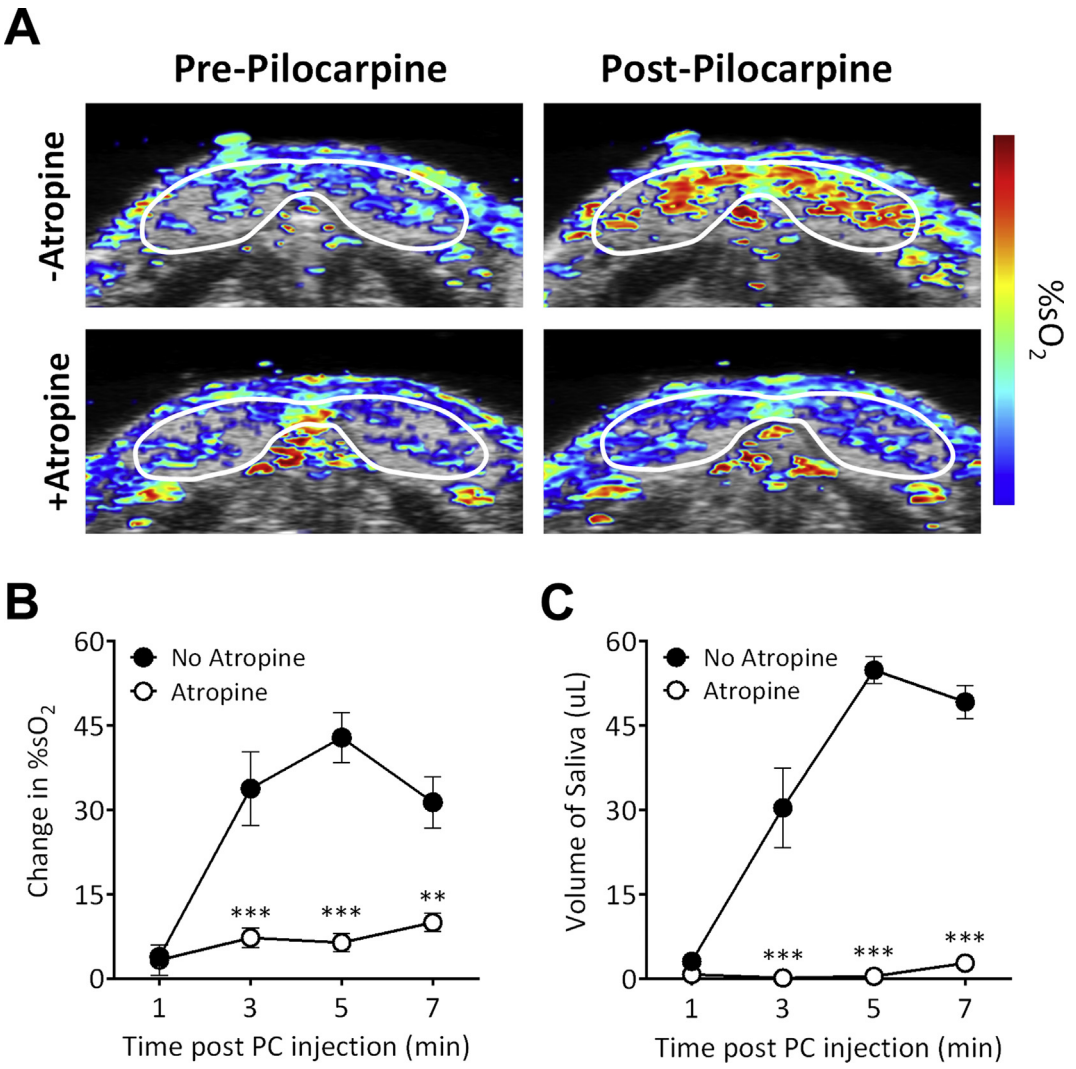

Fig. 3. Effect of atropine on pilocarpine-induced hemodynamic response in salivary glands. (A) Pseudo-colorized $\%sO_2$ maps of salivary glands acquired before (Pre-Pilocarpine) and after pilocarpine (Post-Pilocarpine) administration with or without atropine. A visual loss in hemodynamic response to pilocarpine stimulation was observed after atropine treatment (+Atropine). (B) Quantitative measure of change in salivary gland %sO2 levels showed a significant reduction in animals pre-treated with atropine compared to animals treated with pilocarpine alone (No atropine). (C) Saliva volume measurements also showed significantly lower salivary secretion levels in atropine treated animals compared to animals treated only with pilocarpine. Error bars represent standard error of the mean. $^{**}p < 0.01$, $^{***}p < 0.001$, $^{****}p < 0.0001$.

salivary glands (parotid, submandibular, and sublingual). This could be important in understanding the heterogeneity in the vascular response of the individual glands to autonomic stimulation and their relative contribution to salivary secretion in mice. Second, we examined the changes in salivary glands following exogenous stimulation or blockade. The potential of PAI for assessment of salivary gland hemodynamics following direct activation of the sympathetic or parasympathetic nerves in response to stress (e.g. physical restraint) remains to be investigated. And finally, given the influence of systemic changes in cardiovascular function on regional blood flow, studies should also examine the impact of changes in heart rate or blood pressure on salivary gland blood flow.

Ethical approval statement

All experimental procedures were performed under aseptic conditions and in accordance with protocols approved by the Institutional Animal Care and Use Committee at Roswell Park Comprehensive Cancer Center.

Acknowledgements

The authors thank Adam Killeen, Nicole Kennard, and the staff from the following shared resources at Roswell Park Comprehensive Cancer Center for their assistance in performing the experiments: Laboratory Animal Shared Resource, Translational Imaging Shared Resource, and the Pathology Network Shared Resource.

Conflicts of interest

The authors declare no competing financial interests. The funding sponsors had no role in the design of the study, collection, analyses, or interpretation of data, writing of the manuscript, and in the decision to publish the results.

Funding

This work was supported by grants from the National Cancer Institute 1R01CA204636, National Center for Research Resources S10OD010393, and the Alliance Foundation of Western New York

(all to M.S), and utilized shared resources supported by Roswell Park's Cancer Center Support Grant from the National Cancer Institute P30CA06156.

Appendix A. Supplementary data

Supplementary data to this article can be found online at https://doi.org/10.1016/j.job.2019.08.002.

References

[1] Edgar WM. Saliva: its secretion, composition and functions. Br Dent J 1992;172:305–12.
[2] Dawes C, Pedersen AM, Villa A, Ekström J, Proctor GB, Vissink A, Aframian D, McGowan R, Aliko A, Narayana N, Sia YW, Joshi RK, Jensen SB, Kerr AR, Wolff A. The functions of human saliva: a review sponsored by the World Workshop on Oral Medicine VI. Arch Oral Biol 2015;60:863–74.
[3] Proctor GB, Carpenter GH. Regulation of salivary gland function by autonomic nerves. Auton Neurosci 2007;133:3–18.
[4] Emmelin N. Nerve interactions in salivary glands. J Dent Res 1987;66:509–17.
[5] Proctor GB. The physiology of salivary secretion. Periodontol 2000;2016(70): 11–25.
[6] Holsinger FC, Bui DT. Anatomy, function, and evaluation of the salivary glands. In: Myers EN, Ferris RL, editors. Salivary gland disorders. Berlin, Heidelberg: Springer Berlin Heidelberg; 2007. p. 16.
[7] Bloom SR, Edwards AV, Garrett JR. Effects of stimulating the sympathetic innervation in bursts on submandibular vascular and secretory function in cats. J Physiol 1987;393:91–106.
[8] Lung MA. Mechanisms of sympathetic enhancement and inhibition of parasympathetically induced salivary secretion in anaesthetized dogs. Br J Pharmacol 1994;112:411–6.
[9] Ekström J, Khosravani N, Castagnola M, Messana I. Saliva and the control of its secretion. In: Ekberg O, editor. Dysphagia. Medical Radiology. Cham: Springer; 2017. p. 21–57.
[10] Lung MA. Variations in blood flow on mandibular glandular secretion to autonomic nervous stimulations in anaesthetized dogs. J Physiol 1990;431:479–93.
[11] Anderson LC, Garrett JR. Neural regulation of blood flow in the rat submandibular gland. Eur J Morphol 1998;36(Suppl):3–8.
[12] Edwards AV, Garrett JR. Nitric oxide-related vasodilator responses to parasympathetic stimulation of the submandibular gland in the cat. J Physiol 1993;464:379–92.
[13] Stojic D, Terzic M. Oxygen consumption mediated by M2 muscarinic receptors in rat salivary glands. J Dent Res 1987;66:1435–7.
[14] Sakamoto S, Ichikawa S, Kombayashi T, Tsuboi M. Effects of adrenaline, noradrenaline and pilocarpine on the oxygen uptake in rat submandibular gland. Nihon Seirigaku Zasshi 1981;43:469–78.
[15] Kruger RA. Photoacoustic ultrasound. Med Phys 1994;21:127–31.
[16] Laufer J, Delpy D, Elwell C, Beard P. Quantitative spatially resolved measurement of tissue chromophore concentrations using photoacoustic spectroscopy: application to the measurement of blood oxygenation and haemoglobin concentration. Phys Med Biol 2007;52:141–68.
[17] Li C, Wang LV. Photoacoustic tomography and sensing in biomedicine. Phys Med Biol 2009;54:R59–97.
[18] Bialek EJ, Jakubowski W, Zajkowski P, Szopinski PT, Osmolski A. US of the major salivary glands: anatomy and spatial relationships, pathologic conditions, and pitfalls. RadioGraphics 2006;26:745–63.
[19] Carotti M, Ciapetti A, Jousse-Joulin S, Salaffi F. Ultrasonography of the salivary glands: the role of grey-scale and colour/power Doppler. Clin Exp Rheumatol 2014;32(Supplement 1):S61–70.
[20] Rich LJ, Seshadri M. Photoacoustic imaging of salivary glands. Biomed Opt Express 2015;6:3157–62.
[21] Berggreen E, Nyløkken K, Delaleu N, Hajdaragic-Ibricevic H, Jonsson MV. Impaired vascular responses to parasympathetic nerve stimulation and muscarinic receptor activation in the submandibular gland in nonobese diabetic mice. Arthritis Res Ther 2009;11:R18.
[22] Ono K, Inagaki T, Iida T, Wakasugi-Sato N, Hosokawa R, Inenaga K. Distinct effects of cevimeline and pilocarpine on salivary mechanisms, cardiovascular response and thirst sensation in rats. Arch Oral Biol 2012;57:421–8.
[23] Smaje LH, Gamble J. Transcapillary transport during secretion by the rabbit submandibular salivary gland. J Dent Res 1987;66:564–8.
[24] Fazekas A, Gazelius B, Edwall B, Theodorsson-Norheim BE, Blomquist L, Lundberg JM. VIP and noncholinergic vasodilatation in the rabbit submandibular gland. Peptides 1987;8:13–20.
[25] Ariji Y, Yuasa H, Ariji E. High-frequency color Doppler sonography of the submandibular gland: relationship between salivary secretion and blood flow. Oral Surg Oral Med Oral Pathol Oral Radiol Endod 1998;86: 476–81.